Bioorganic & Medicinal Chemistry 19 (2011) 102–110

Contents lists available at ScienceDirect

Bioorganic & Medicinal Chemistry

journal homepage: www.elsevier.com/locate/bmc

Synthesis and evaluation of 6-[1-(2-[^{18}F]fluoro-3-pyridyl)-5-methyl-1*H*-1,2,3-triazol-4-yl]quinoline for positron emission tomography imaging of the metabotropic glutamate receptor type 1 in brain

Masayuki Fujinaga [a], Tomoteru Yamasaki [a], Kazunori Kawamura [a], Katsushi Kumata [a], Akiko Hatori [a], Joji Yui [a], Kazuhiko Yanamoto [a], Yuichiro Yoshida [a,b], Masanao Ogawa [a,b], Nobuki Nengaki [a,b], Jun Maeda [a], Toshimitsu Fukumura [a], Ming-Rong Zhang [a,*]

[a] *Molecular Imaging Center, National Institute of Radiological Sciences, 4-9-1 Anagawa, Inage-ku, Chiba 263-8555, Japan*
[b] *SHI Accelerator Service Co. Ltd, 5-9-11 Kitashinagawa, Shinagawa-ku, Tokyo 141-8686, Japan*

ARTICLE INFO

Article history:
Received 27 September 2010
Revised 18 November 2010
Accepted 20 November 2010
Available online 25 November 2010

Keywords:
Metabotropic glutamate receptor type 1
[^{18}F]FPTQ
Autoradiography
PET

ABSTRACT

The purpose of this study was to synthesize 6-[1-(2-[^{18}F]fluoro-3-pyridyl)-5-methyl-1*H*-1,2,3-triazol-4-yl]quinoline ([^{18}F]FPTQ, [^{18}F]**7a**) and to evaluate its potential as a positron emission tomography ligand for imaging metabotropic glutamate receptor type 1 (mGluR1) in the rat brain. Compound [^{18}F]**7a** was synthesized by [^{18}F]fluorination of 6-[1-(2-bromo-3-pyridyl)-5-methyl-1*H*-1,2,3-triazol-4-yl]quinoline (**7b**) with potassium [^{18}F]fluoride. At the end of synthesis, 1280–1830 MBq (n = 8) of [^{18}F]**7a** was obtained with >98% radiochemical purity and 118–237 GBq/μmol specific activity using 3300–4000 MBq of [^{18}F]F^-. In vitro autoradiography showed that [^{18}F]**7a** had high specific binding with mGluR1 in the rat brain. Biodistribution study using a dissection method and small-animal PET showed that [^{18}F]**7a** had high uptake in the rat brain. The uptake of radioactivity in the cerebellum was reduced by unlabeled **7a** and mGluR1-selective ligand JNJ-16259685 (**2**), indicating that [^{18}F]**7a** had in vivo specific binding with mGluR1. Because of a low amount of radiolabeled metabolite present in the brain, [^{18}F]**7a** may have a limiting potential for the in vivo imaging of mGluR1 by PET.

1. Introduction

Metabotropic glutamate receptors (mGluRs) are a family of G-protein coupled receptors activated by the neurotransmitter glutamate.[1,2] These receptors have been divided into three groups with eight subtypes based on their pharmacology, signal transduction mechanism, and sequence homology. Group I mGluRs, including mGluR1 and mGluR5, modulate intracellular calcium by stimulating phospholipase C and regulate neuronal excitability.[3,4] MGluR1 is mainly a postsynaptic receptor and may be related to diseases such as stroke, epilepsy, pain, cerebellar ataxia, Parkinson's disease, anxiety, and mood disorders.[4–7] To elucidate the physiological role of mGluR1 in the brain and the therapeutic potential of mGluR1 ligands[8–14] in the pathology and/or etiology of central nervous system diseases, radioligands (Scheme 1) labeled with a positron-emitting radioisotope have been developed to visualize mGluR1 in living brains using positron emission tomography (PET).

As the first PET ligand for mGluR1, [^{11}C]JNJ-16567083 ([^{11}C]**1**, K_i = 0.87 nM for mGluR1) was developed for imaging this receptor in the rodent brain.[15] Compound [^{11}C]**1** is an analog of JNJ-16259685 (**2**, K_i = 0.34 nM), a potent mGluR1 antagonist.[16] Compound [^{11}C]**1** had high uptake of radioactivity in the rat cerebellum, which is a region with high density of mGluR1;[17,18] however, further evaluation, including clinical investigation using [^{11}C]**1**, has not been reported. Recently, two ^{18}F-labeled triazole analogs [^{18}F]MK-1312 ([^{18}F]**3**, K_i = 0.40 nM)[19] and [^{18}F]FTIDC ([^{18}F]**4**, K_i = 3.9 nM)[20,21] for imaging mGluR1 have been presented at two meetings. Compound [^{18}F]**3** and [^{18}F]**4** were shown to have high uptake in the brains of monkeys and rats, respectively.[19,21] Further characterization demonstrated that [^{18}F]**3** had in vivo specific binding with mGluR1 in the monkey brain.[22] In addition, a preliminary study reported that [^{11}C]MMTP ([^{11}C]**5**, K_i = 7.9 nM) showed a specific location of radioactivity in the cerebellum of the monkey brain.[23]

Recently, we have labeled a mGluR1 antagonist YM-202074 (**6**, K_i = 4.8 nM)[24] with ^{11}C and evaluated its potential as a PET ligand for mGluR1.[25] In vitro autoradiographic study demonstrated that [^{11}C]**6** had high specific binding with mGluR1 in the rat cerebellum and its regional distribution was consistent with the distribution pattern of mGluR1 in the brain. However, the brain uptake of [^{11}C]**6** was very low, which hampered its usefulness for in vivo imaging.

* Corresponding author. Tel.: +81 43 382 3708; fax: +81 43 206 3261.
E-mail address: zhang@nirs.go.jp (M.-R. Zhang).

0968-0896/$ - see front matter © 2010 Elsevier Ltd. All rights reserved.
doi:10.1016/j.bmc.2010.11.048

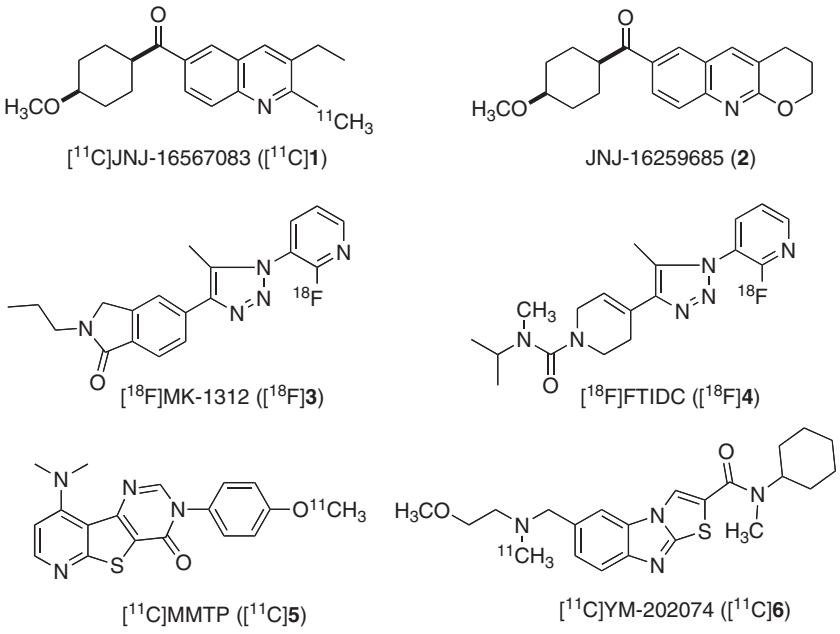

Scheme 1. Chemical structures of ligands for mGluR1.

To develop a PET ligand with improved properties compared to [^{11}C]**6** for imaging mGluR1 in the brain, we established 6-[1-(2-fluoro-3-pyridyl)-5-methyl-1*H*-1,2,3-triazol-4-yl]quinoline (FPTQ, **7a**; Scheme 2) as a target compound in the present study. Compound **7a** had a potent in vitro binding affinity (IC_{50} = 3.6 nM and 1.4 nM for human and mouse mGluR1), but its chemical synthesis has not been reported.[26,27] In this study, we synthesized and evaluated [^{18}F]FPTQ ([^{18}F]**7a**) as a promising PET ligand for mGluR1. Here, we report: (1) the chemical synthesis of unlabeled **7a** and a novel bromo precursor **7b** for labeling, (2) the radiosynthesis of [^{18}F]**7a**, and (3) the in vitro and in vivo characterization of [^{18}F]**7a** for mGluR1 in the rat brain.

2. Results

2.1. Chemical synthesis

The two triazole analogs **7a** and **7b** were synthesized according to the reaction sequences lineated in Scheme 3. 3-Azido-2-fluoropyridine (**8a**) was prepared by reacting 2-fluoropyridine with lithium diisopropylamide (LDA) and then an azide agent at −78 °C for 1 h. Cyclization of **8a** with tributyl(1-propynyl)tin in toluene produced **9a** with a triazole ring. Coupling of **9a** with quinolinyltriflate **10** in the presence of tetrakis(triphenylphosphine)palladium as a catalyst at 80 °C gave **7a**. The overall chemical yield of **7a** was 21% from 2-fluoropyridine.

3-Amino-2-bromopyridine was first treated with sodium nitrite and tetrafluoroboric acid, followed by substitution with sodium azide to give azidobromopyridine **8b**. As with **8a**, **8b** was reacted with the alkynyl regent to afford triazole **9b**. The novel bromo precursor **7b** was prepared by coupling of **9b** with **10** with a total yield of 33% from aminobromopyridine.

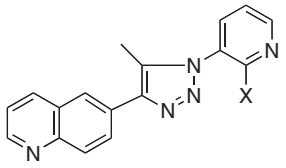

Scheme 2. Chemical structures of unlabeled **7a** and [^{18}F]**7a** for mGluR1 in this study.

2.2. Radiosynthesis

Compound [^{18}F]**7a** was synthesized by heating the bromo precursor **7b** with cyclotron-produced potassium [^{18}F]fluoride ([^{18}F]KF) in anhydrous DMSO at 150 °C for 10 min (Scheme 3). After the [^{18}F]fluorination reaction, semi-preparative HPLC purification of the reaction mixture gave [^{18}F]**7a** in 69 ± 13% (n = 8) radiochemical yields based on [^{18}F]F^-, corrected for physical decay for an averaged synthesis time of 75 min (Fig. 1A). The identity of [^{18}F]**7a** was confirmed by coinjection with unlabeled **7a** on analytic HPLC. At the end of synthesis (EOS), the radiochemical purity and specific activity of [^{18}F]**7a** was higher than 99% (Fig. 1B) and 118–237 GBq/mmol, respectively. No significant peak corresponding to unreacted **7b** or other chemical impurities was observed on the HPLC chart of the final product (Fig. 1B). The radiochemical purity of [^{18}F]**7a** remained higher than 95% after maintaining the formulated product for at least 3 h at room temperature.

2.3. Computation of *c* Log *P* and *c* Log *D*, and measurement of Log *D*

The computed values of *c* Log *P* and *c* Log *D* (at pH 7.4) for **7a** were 2.93 and 3.05, respectively. The measured Log *D* value of [^{18}F]**7a** was 2.53 ± 0.02 (n = 3).

2.4. In vitro autoradiography

Figure 2 and Table 1 show representative in vitro autoradiograms and quantitative results of the [^{18}F]**7a** binding in the brain sections of rats (n = 4). The distribution pattern of [^{18}F]**7a** was heterogenous with high radioactivity in the cerebellum, a known mGluR1-rich region (A). The thalamus displayed a moderate level of radioactivity. Low radioactivity was seen in the hippocampus, striatum, olfactory bulb, cerebral cortex, and pons-medulla (Table 1). Incubation with unlabeled **7a** (B) and mGluR1 antagonist 2 (C) at 1 μM markedly decreased the radioactivity in the brain sections to <3% of total radioactivity (Table 1), respectively. On the other hand, MPEP

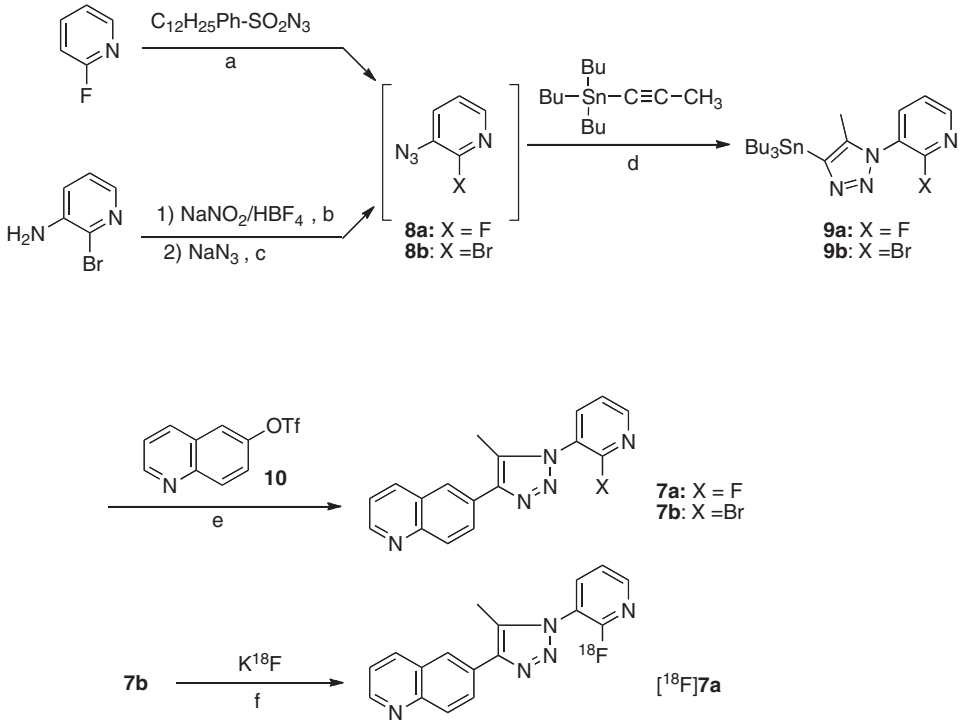

Scheme 3. Chemical synthesis and radiosynthesis. Reagents and conditions: (a) lithium diisopropylamide, THF, −78 °C, 1 h; (b) 0 °C, 2 h; (c) 0 °C, 2 h; (d) toluene, reflux, 12 h, 42% (**9a**), 64% (**9b**); (e) $Pd(PPh_3)_4$, CsF, CuI, DMF, 80 °C, 12 h, 49% (**7a**), 52% (**7b**); (f) DMSO, 150 °C, 10 min, 69% decay-corrected based on total $[^{18}F]F^-$.

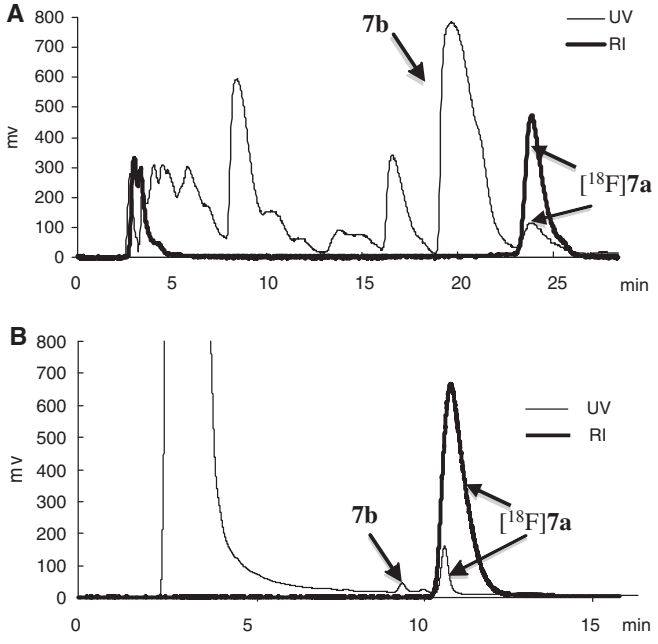

Figure 1. Chromatograms from the HPLC separation (A) and analysis (B) used in the radiosynthesis of [^{18}F]**7a**. See Section 5 for chromatographic conditions.

(a mGluR5 antagonist) at 1 μM did not reduce the radioactivity in the cerebellum, thalamus, hippocampus, olfactory bulb, and striatum (D, Table 1), although MPEP at 10 μM decreased the binding to 30–40% of total binding in all regions examined (E).

2.5. Biodistribution by dissection

The radioactivity distribution was measured in rats (n = 3) at 5, 15, and 30 min after injection of [^{18}F]**7a** (Table 2). The radioactivity values in most tissues were the highest at 5 min and thereafter decreased quickly. High uptake was found in the liver and small intestine, while low uptake was determined in the blood and other peripheral organs, including the heart, lung, spleen, kidney, pancreas, and muscle. On the other hand, relatively high radioactivity was detected in the brain, the target tissue of this study. Among all brain regions examined, the cerebellum showed the highest uptake. The radioactivity in the thalamus was lower than that in the cerebellum, but was slightly higher than that in the hippocampus, striatum, cerebral cortex, olfactory bulb, and pons-medulla.

2.6. Small-animal PET imaging

Figures 3A–D and 4A show representative PET/MRI-fused brain images and time–activity curves (TACs) of [^{18}F]**7a** in the brain regions of rats. The summation images (A and B) between 0 and 30 min after radioligand injection showed the highest uptake of radioactivity in the cerebellum. A lower but detectable radioactivity level was seen in the thalamus (C), hippocampus (C), striatum (D), and cerebral cortex (D). The lowest uptake was found in the medulla (A and B), a region with low mGluR1 density. As shown in the TACs (Fig. 4A), [^{18}F]**7a** entered the brain rapidly after injection and radioactivity peaked at 1–3 min in all regions examined. The maximum uptakes were 2.3 standard uptake value (SUV) in the cerebellum, 2.1 SUV in the thalamus, and 1.1–1.5 SUV in the hippocampus, striatum, cerebral cortex, and medulla, respectively. After the initial uptake, the radioactivity level in the cerebellum at 15 and 30 min decreased to 66% and 37% of the maximum. Compared to the cerebellum, other regions showed a faster decrease in radioactivity. From 20 min after injection, radioactivity in the regions except the cerebellum remained at a similar and low level. The uptake ratio of radioactivity in the regions to that in the medulla was used as an index to reflect in vivo specific binding of [^{18}F]**7a** in the brain. The uptake ratio of each region/medulla was 3.73 ± 0.50 (n = 4) for the cerebellum, 1.91 ± 0.15 for the thalamus,

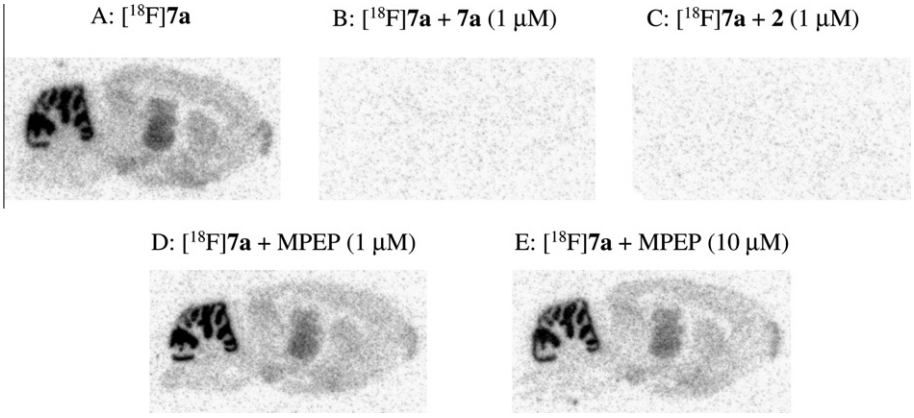

Figure 2. Representative in vitro autoradiograms of [^{18}F]**7a** in brain sections. (A) [^{18}F]**7a** alone; (B) [^{18}F]**7a** with **7a** (1 μM); (C) [^{18}F]**7a** with **2** (1 μM); (D) [^{18}F]**7a** with MPEP (1 μM); (E) [^{18}F]**7a** with MPEP (10 μM).

Table 1
Regional distribution of [^{18}F]**7a** in rat brain sections determined by in vitro autoradiography

Region	Radioactivity[a] (PSL/mm^2)				
	[^{18}F]7a	mGluRl antagonists		mGluR5 antagonists	
		7a (1 μM)	(1 μM)	MPEP (1 μM)	MPEP (10 μM)
Cerebellum	408.8 ± 48.1	—[b]	—[b]	397.5 ± 31.6	284.7 ± 41.4*
Thalamus	188.9 ± 44.4		—	169.4 ± 39.9	115.7 ± 20.7*
Hippocampus	112.4 ± 29.4		—	97.4 ± 27.7	69.4 ± 13.1*
Olfactory bulb	88.7 ± 38.1		—	76.0 ± 30.7	49.0 ± 16.9*
Striatum	70.7 ± 14,2		—	61.7 ± 16.0	40.1 ± 6.9*
Cerebral cortex	28.2 ± 4.7		—	23.6 ± 4.2*	15.7 ± 3.3*
Pons-medulla	17.5 ± 2.7			15.2 ± 2.5*	9.5 ± 1.7*
Whole brain		0.6 ± 0.2[c]	0.5 ± 0.2[c]	—[b]	—[b]

[a] Radioactivity concentrations in regions of interest (ROIs) were expressed as photo-stimulated luminescence values (PSL)/area (mm^2). Data are the means ± SD (n = 6–8 in each group).
[b] Not determined.
[c] In the presence of **7a** or **2**, ROIs were placed on the whole brain.
* P <0.05 (Student's paired t-test, compared with [^{18}F]**7a** alone).

Table 2
Biodistribution of [^{18}F]**7a** in rats (n = 3) by dissection method

Tissues	5 min	15 min	30 min
Blood	0.38 ± 0.01	0.26 ± 0.04	0.15 ± 0.05
Heart	0.47 ± 0.03	0.24 ± 0.05	0.16 ± 0.07
Lung	0.50 ± 0.03	0.31 ± 0.06	0.17 ± 0.09
Liver	2.30 ± 0.35	2.04 ± 0.29	1.93 ± 0.20
Spleen	0.43 ± 0.03	0.25 ± 0.05	0.16 ± 0.10
Kidney	0.76 ± 0.06	0.57 ± 0.06	0.39 ± 0.14
S. intestine	3.06 ± 1.22	4.64 ± 1.39	1.74 ± 0.35
Pancreas	0.75 ± 0.03	0.34 ± 0.12	0.21 ± 0.14
Muscle	0.28 ± 0.01	0.14 ± 0.04	0.10 ± 0.06
Bone	0.22 ± 0.02	0.15 ± 0.02	0.22 ± 0.05
Whole brain	0.52 ± 0.01	0.23 ± 0.04	0.11 ± 0.03
Cerebellum	1.21 ± 0.05	0.54 ± 0.09	0.20 ± 0.03
Hippocampus	0.58 ± 0.02	0.22 ± 0.05	0.09 ± 0.03
Thalamus	0.73 ± 0.05	0.29 ± 0.02	0.10 ± 0.03
Striatum	0.54 ± 0.06	0.23 ± 0.04	0.11 ± 0.04
Olfactory bulb	0.52 ± 0.06	0.24 ± 0.08	0.10 ± 0.02
Cerebral cortex	0.44 ± 0.00	0.20 ± 0.04	0.09 ± 0.03
Pons-medulla	0.47 ± 0.01	0.21 ± 0.04	0.13 ± 0.10

1.55 ± 0.22 for the striatum, 1.42 ± 0.11 for the hippocampus, and 1.31 ± 0.13 for the cerebral cortex between 10 and 15 min after injection.

As shown in PET images (Fig. 3E–H) and TACs (Fig. 4B), pretreatment with unlabeled **7a** (1.0 mg/kg) led to a remarked reduction in the uptake compared to the control group. With this treatment, the radioactivity distribution became fairly uniform in the whole brain. The radioactivity in the cerebellum was reduced to about 30% of the control, while that in the thalamus, hippocampus, striatum, and cerebral cortex was decreased to 50–70% of the control. Similar to **7a**, mGluR1-selective **2** also reduced the uptake and diminished the difference in radioactivity among all brain regions (Figs. 3I–L and 4C). On the other hand, pretreatment with MPEP did not change the distribution of [^{18}F]**7a** in the brain (Figs. 3M–P and 4D). The difference in the TACs of the same brain regions between the control and MPEP-treatment groups was analyzed by two-way repeated-measures ANOVA. This comparison showed that difference in the cerebellum was not significant (P = 0.86), but difference in the thalamus, hippocampus, striatum, and cerebral cortex was statistically significant (P <0.05).

2.7. Metabolite analysis

Figure 5 shows the percentages of parent [^{18}F]**7a** in the cerebellum, the brain except the cerebellum, and the plasma of mouse measured by analytical HPLC with a detector for radioactivity. The fraction corresponding to parent [^{18}F]**7a** (retention time: 5.8 min) in the plasma rapidly decreased to 57% at 5 min, to 23% at 15 min, and to 4% at 30 min after injection. A major radiolabeled metabolite (retention time: 2.7 min) with high polarity was observed on the HPLC charts. On the other hand, parent [^{18}F]**7a** in the cerebellum homogenate remained at 91% of total radioactivity at 15 min after injection. The percentages of parent [^{18}F]**7a** were 67% and 34% of total radioactivity in the cerebellum and brain except the cerebellum at 30 min, respectively.

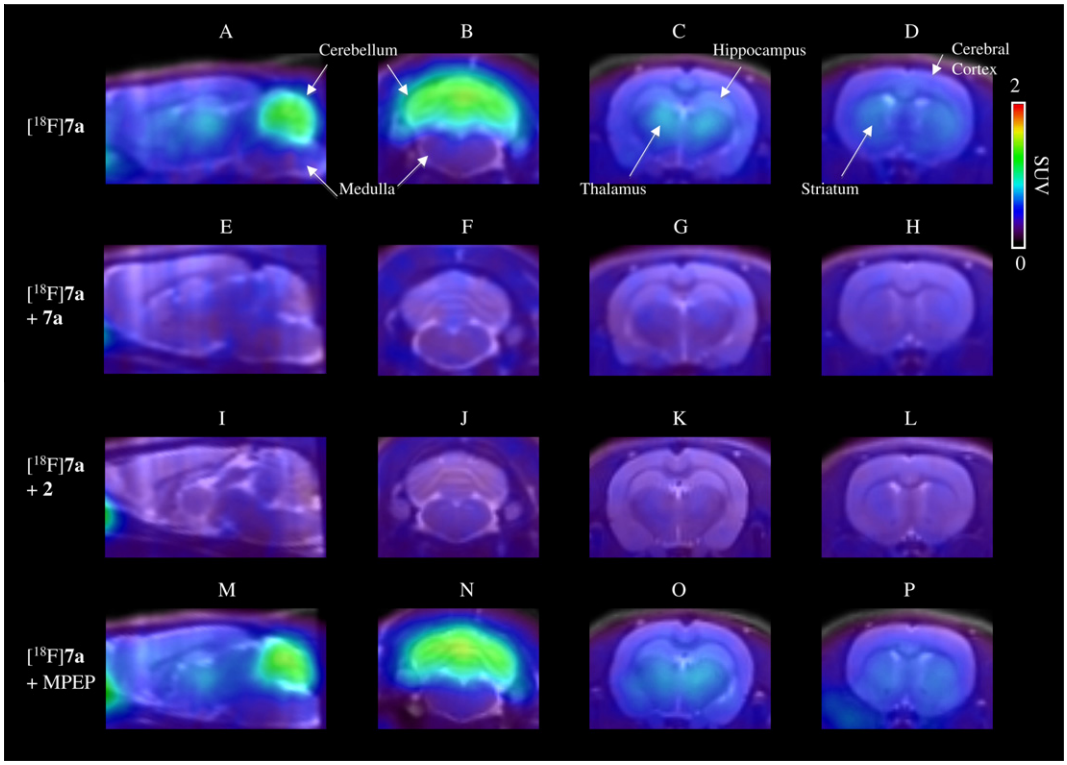

Figure 3. Representative PET/MRI-fused images of [^{18}F]**7a** in the isoflurane-anesthetized rat brains. PET images were generated by summing the whole scan (0–30 min) and were overlaid on MRI images of anatomical templates. (A–D) [^{18}F]**7a** alone; (E–H) [^{18}F]**7a** after treatment with **7a** (1 mg/kg); (I–L) [^{18}F]**7a** after treatment with **2** (1 mg/kg); (M–P) [^{18}F]**7a** after treatment with MPEP (1 mg/kg). (A, E, I, M) sagittal images; left numbers: coronal images.

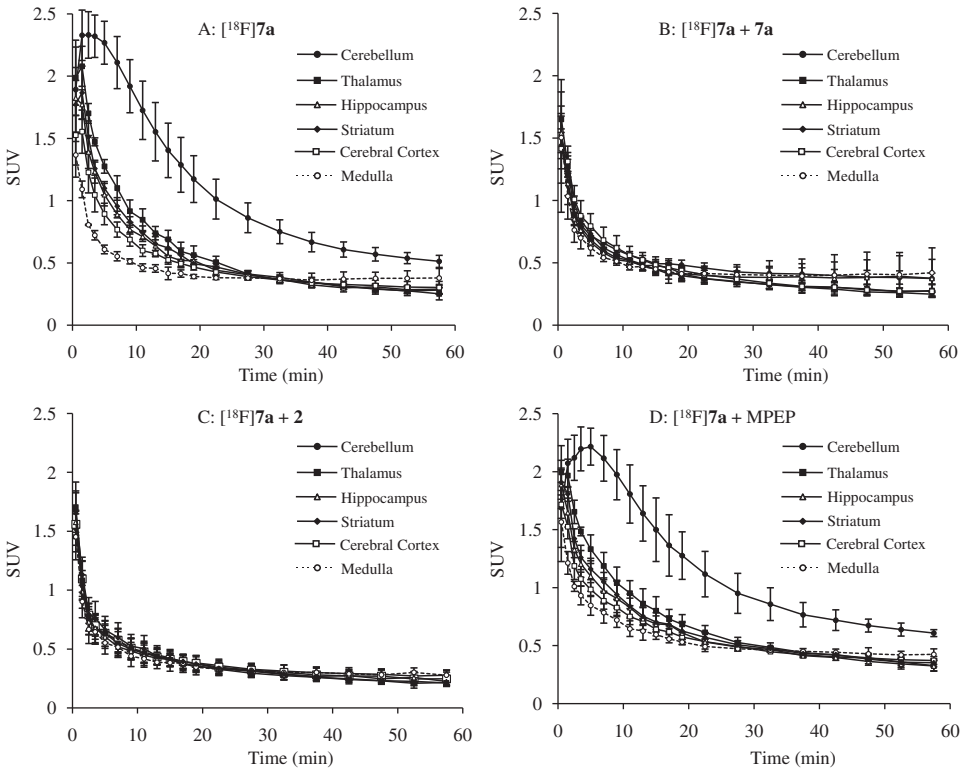

Figure 4. Time–activity curves in the rat brain regions after injection of [^{18}F]**7a**. (A) [^{18}F]**7a** alone; (B) [^{18}F]**7a** after treatment with **7a** (1 mg/kg); (C) [^{18}F]**7a** after treatment with **2** (1 mg/kg); (D) [^{18}F]**7a** after treatment with MPEP (1 mg/kg). The uptakes of radioactivity were decay-corrected to the injection time and are expressed as the standardized uptake value (SUV), normalized for injected radioactivity and body weight. Data are the means ± SD (n = 4 in each group).

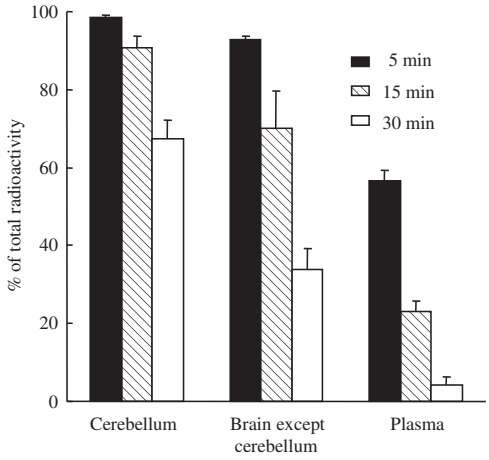

Figure 5. Metabolite analysis of [^{18}F]**7a** in the cerebellum, brain except the cerebellum, and plasma of mice (n = 3 in each group).

2.8. Protein binding

The binding of [^{18}F]**7a** with protein in the plasma was determined by ultra-filtration. The free (not protein-bound) fraction was 8.5–9.9%.

3. Discussion

In this study, we synthesized [^{18}F]**7a** and determined its in vitro and in vivo specific binding with mGluR1 in the rat brain using autoradiography and small-animal PET.

We described the synthetic route of unlabeled **7a**, which was adapted from the patent literature[26] and is the first full report of its reaction, purification, and characterization data. We prepared **7a** by three-step reactions using commercially available materials (Scheme 3). By treating fluoropyridine with LDA and then an azide reagent, the azide group was successfully introduced to the pyridine ring to give **8a**. However, this introducing route is not suitable for the synthesis of bromo **8b**, which is a key intermediate for preparing the novel bromo precursor **7b**. Because LDA is a strong base and would have caused the lithiodebromination of 2-bromopyridine, we determined another approach instead of using LDA. After aminobromopyridine was diazonized, treatment of the reaction mixture with sodium azide afforded **8b**. Unstable **8a** or **8b** was not purified and was directly used for cyclization. Subsequent coupling of **9a** or **9b** with triflate **10** produced the desired **7a** or **7b**.

Since **7a** structurally has a fluorine atom attached to the 2-posion of the pyridine ring, this compound is easily labeled with ^{18}F by nucleophilic [^{18}F]fluorination. This labeling did not change the chemical structure and pharmacological profile of **7a**. [^{18}F]Fluorination of the bromo precursor **7b** proceeded efficiently to give [^{18}F]**7a**, which could be separated from the unreacted precursor by prolonging their retention times (**7b**: 19.6 min; [^{18}F]**7a**: 23.7 min) during the HPLC purification (Fig. 1). At EOS, the radioactivity amount, radiochemical purity, stability, and specific activity of [^{18}F]**7a** were sufficient for animal experiments.

The measured Log D value of [^{18}F]**7a** was found to be 2.53 and was appreciably different from the computed value (3.05). The measured value lies in the range normally considered favorable for good penetration of the blood–brain barrier (BBB) in the absence of any effect of efflux transporters.[28]

In vitro autoradiographic results (Fig. 2, Table 1) showed that the distribution pattern of [^{18}F]**7a** in the brain regions was consistent with the distribution of mGluR1 reported previously.[17,18] In vitro study using a selective radioligand [^{3}H]R214127[18] for mGluR1 in the rat brain showed the highest density of mGluR1 in the cerebellum, moderate density in the thalamus, hippocampus, and olfactory bulb, and low density in the cerebral cortex, striatum, and pons-medulla. The present distribution of [^{18}F]**7a** in the rat brain was similar to that of [^{3}H]R214127 or [^{11}C]**6**.[25] Although the radioactivity level was different among the brain regions examined, the specific binding of [^{18}F]**7a** accounted for higher than 97% of total binding, as determined by incubating with unlabeled **7a** or mGluR1-selective **2**. On the other hand, mGluR5-selective MPEP (IC_{50}: 10 nM for mGluR5 and >10 mM for mGluR1)[10] at 10 mM decreased the binding to 30–40% of the control, suggesting that [^{18}F]**7a** may have a very weak affinity with mGluR5 (IC_{50} >10 μM) based on this in vitro autoradiography. However, MPEP at 1 μM did not inhibit the binding in most regions with statistical significance. This autoradiography demonstrated that [^{18}F]**7a** has high in vitro binding for mGluR1 in the rat cerebellum.

Dissection method and small-animal PET were used to determine the in vivo distribution of [^{18}F]**7a** in the rat. Compound [^{18}F]**7a** had high uptake in the liver and small intestine, suggesting that the hepatability and urinary excretion, as well as intestinal reuptake pathway dominated the whole-body distribution of [^{18}F]**7a** and a rapid washout of radioactivity from the body (also see TACs of peripheral organs described in Supplementary data). The brain uptake of [^{18}F]**7a** was relatively high, indicating that this radioligand passes across the BBB and enters the brain, which is a prerequisite for a favorable PET ligand used in brain imaging. This uptake was probably related to the suitable lipophilicity (Log D: 2.53) of [^{18}F]**7a** and relatively high percentage (8.5–9.9%) of free fraction in the plasma. Regional distribution of [^{18}F]**7a** in the brain was heterogeneous and the highest radioactivity was detected in the cerebellum among all brain regions (Table 2).

PET imaging showed that the distribution and uptake of [^{18}F]**7a** in the brain was consistent with the results obtained by dissection as well as by in vitro autoradiography. The uptake of [^{18}F]**7a** in the cerebellum was fivefold higher than that of [^{11}C]**6**[25] in the rat cerebellum, and was similar to that of [^{18}F]**3**[19] in the monkey cerebellum, although the level was approximately 1/3 that of [^{11}C]**1**.[15] Pretreatment with **7a** (Figs. 3E–H and 4B) and **2** (Figs. 3I–L and 4C) significantly reduced the uptake and completely diminished the difference in uptakes among all brain regions. The obvious blockade by **7a** and **2** showed that the binding in the receptor-rich cerebellum was mGluR1 mediated. On the other hand, the uptake was not changed in the cerebellum by treatment with mGluR5-selective MPEP, but slightly decreased in the thalamus with statistical significance, suggesting the low specific binding in the thalamus may also be related to mGluR5.

Presence of a radiometabolite in plasma may reduce the specific binding of a parent PET ligand if the radiometabolite enters the brain and is retained/bound at the target sites. Although in vivo metabolite analysis showed the presence of a radiometabolite in the plasma, the main radioactive component in the cerebellum and other regions was parent [^{18}F]**7a** at 15 min after injection (Fig. 5). On the other hand, although defluorination of the [^{18}F]ligand is a possible metabolite route that could hamper brain imaging and quantitative analysis of receptors in the brain,[29] no considerable radioactivity was visualized in the skull, as shown in the present PET images (Fig. 3). Dissection also demonstrated no obvious increase of radioactivity in the bone between 5 and 30 min after injection (Table 2). Thus, despite the presence of a small amount of radiometabolite in the brain, we assumed that the specific binding to mGluR1 determined in the brain until 15 min after radioligand injection was mainly due to parent [^{18}F]**7a**.

4. Conclusions

This study described the synthesis and characterization of a PET ligand [^{18}F]**7a** for imaging mGluR1 in the rat brain. [^{18}F]**7a** was synthesized by [^{18}F]fluorination of the bromo precursor **7b** with [^{18}F]F^- at high and reproducible radiochemical yields. Compound [^{18}F]**7a** exhibited in vitro and in vivo binding with mGluR1 in the brain regions such as the cerebellum, suggesting its usefulness for visualizing mGluR1 in the cerebellum. However, the rapid dissociation of [^{18}F]**7a** in the brain may show limited specificity for mGluR1 and its brain kinetics may be easily influenced by blood flow. Moreover, the presence of a low amount of radiolabeled metabolite in the brain may disturb determination for the specific binding of this radioligand. Thus, [^{18}F]**7a** may be of limited application for in vivo investigation of mGluR1. This problem would be solved by the further development of more potent mGluR1-selective PET ligands with improved pharmacological profiles, such as binding affinity and in vivo metabolism.

5. Experimental section

Melting points were uncorrected. ^{1}H NMR spectra were recorded on a JNM-AL-300 spectrometer (JEOL; Tokyo, Japan) with tetramethylsilane as an internal standard. All chemical shifts (δ) were reported in parts per million (ppm) downfield from the standard. High resolution (HR) FAB-MS was obtained on a JEOL NMS-SX102 spectrometer (JEOL). Column chromatography was performed on Wakogel C-200 (Wako Pure Chem Ind; Osaka, Japan). HPLC was performed using a JASCO HPLC system (JASCO; Tokyo, Japan): effluent radioactivity was monitored using a NaI (Tl) scintillation detector system. Compounds **2**, **6**, and MPEP were purchased from ALEXIS BIOCHEMICALS (San Diego, CA). All chemical reagents of the highest grade commercially available were purchased from Aldrich Chem (Milwaukee, WI) or Wako. Fluorine-18 (^{18}F) was produced using a CYPRIS HM-18 cyclotron (Sumitomo Heavy Industry; Tokyo, Japan). If not otherwise stated, radioactivity was measured with an IGC-3R Curiemeter (Aloka; Tokyo, Japan). All animal experiments were performed according to the recommendations of the Committee for the Care and Use of Laboratory Animals, National Institute of Radiological Sciences (Chiba, Japan). Animals were maintained and handled in accordance with the recommendations of National Institute of Health and the institutional guidelines of National Institute of Radiological Sciences. Sprague–Dawley male rats (220–240 g, 7 weeks) were provided by Japan SLC (Shizuoka, Japan).

5.1. Chemical synthesis

5.1.1. 1-(2-Fluoro-3-pyridyl)-5-methyl-4-tri-*n*-butylstannyl-1*H*-1,2,3-triazole (9a)

Normal butyllithium in hexane (2.4 mL, 1.6 M; 3.8 mmol) was added dropwise to a solution of diisopropylamine (0.53 mL, 3.8 mmol) in THF (5 mL) at −78 °C under N_2 atmosphere. The reaction mixture was stirred at −78 °C for 5 min and then at 0 °C for 5 min. After the mixture was cooled again to −78 °C, a solution of 2-fluoropyridine (0.33 mL, 3.8 mmol) in THF (2 mL) was added and the mixture was stirred for 10 min. To this mixture was added a solution of *n*-dodecylbenzenesulfonyl azide (0.89 g, 2.5 mmol) in THF (3 mL), and the reaction mixture was stirred for 1 h at −78 °C. This mixture was quenched with water and extracted with AcOEt. The organic layer was dried over Na_2SO_4 and the solvent was removed to give crude 3-azido-2-fluoropyridine (**8a**).

Tributyl(1-propynyl)tin (0.91 mL, 3.0 mmol) was successively added to a solution of the above **8a** in dry toluene (20 mL) and the reaction mixture was heated at reflux for 12 h. Removal of toluene under reduced pressure gave a residue, which was purified by chromatography on a silica gel column under hexane/AcOEt (3:1) with Et_3N (1%) to give **9a** (489 mg, 42%) as a brown oil. ^{1}H NMR (300 MHz, $CDCl_3$) δ: 0.90 (9H, t, J = 7.1 Hz), 1.12–1.42 (12H, m), 1.54–1.62 (6H, m), 2.29 (3H, d, J = 2.2 Hz), 7.40–7.45 (1H, m), 7.96–8.02 (1H, m), 8.37–8.39 (1H, m). HRMS (FAB) calcd for $C_{20}H_{34}N_4FSn$: 469.1789; found: 469.1761 (M^+).

5.1.2. 1-(2-Bromo-3-pyridyl)-5-methyl-4-tri-*n*-butylstannyl-1*H*-1,2,3-triazole (9b)

To a suspension of 3-amino-2-bromopyridine (1.04 g, 6.0 mmol) in water (8.0 mL) was added dropwise a solution of sodium nitrite (500 mg, 7.2 mmol) and tetrafluoroboric acid (10 mL, 42%) at 0 °C for 2 h. Sodium azide (19 mg, 0.05 mmol) was added with caution and the mixture was stirred at 0 °C for 2 h. The reaction mixture was quenched with saturated Na_2CO_3 and extracted with AcOEt. The organic layer was washed with water and saturated NaCl, and dried over Na_2SO_4. The solvent was removed to give crude 3-azido-2-bromopyridine (**8b**).

Tributyl(1-propynyl)tin (1.16 mL, 2.31 mmol) was successively added to a solution of the above **8b** in dry toluene (10 mL) and the reaction mixture was heated at reflux for 12 h. Removal of toluene under reduced pressure gave a residue, which was chromatographed on silica gel under hexane/AcOEt (3:1) with Et_3N (1%) to afford **9b** (2.03 g, 64%) as a yellowish oil. ^{1}H NMR ($CDCl_3$) δ: 0.90 (9H, t, J = 7.1 Hz), 1.12–1.39 (12H, m), 1.55–1.63 (6H, m), 2.22 (3H, s), 7.47–7.51 (1H, m), 7.73–7.77 (1H, m), 8.55–8.57 (1H, m). HRMS (FAB) calcd for $C_{20}H_{34}N_4BrSn$: 529.0989; found: 529.1019 (M^+).

5.1.3. Quinoline-6-yl trifluoromethanesulfonate (10)

Trifluoromethane sulfonic anhydride (1.40 mL, 8.5 mmol) was added dropwise to a solution of 6-quinolinol (1.01 g, 7.0 mmol) and pyridine (1.1 mL, 14.0 mmol) in CH_2Cl_2 (35 mL) at 0 °C under N_2 atmosphere. The reaction mixture was stirred at room temperature overnight. Removal of CH_2Cl_2 under reduced pressure gave a residue, which was purified by chromatography on a silica gel column using CH_2Cl_2 with Et_3N (1%) to give **10** (1.40 g, 72%) as a yellow solid; mp: 33–34 °C. ^{1}H NMR (300 MHz, $CDCl_3$) δ: 7.50–7.54 (m, 1H), 7.62 (1H, dd, J = 2.7, 9.2 Hz), 7.77 (1H, d, J = 2.6 Hz), 8.22 (2H, d, J = 9.2 Hz), 9.00–9.02 (1H, m). HRMS (FAB) calcd for $C_{10}H_7O_3NF_3S$: 278.0099; found: 278.0083 (M^+).

5.1.4. 6-[1-(2-Fluoro-3-pyridyl)-5-methyl-1*H*-1,2,3-triazol-4-yl]quinoline (7a)

A mixture of **9a** (481 mg, 1.0 mmol), **10** (277 mg, 1.0 mmol), tetrakis(triphenylphosphine)palladium (0) (58 mg, 0.05 mmol), cesium fluoride (304 mg, 2.0 mmol), and copper (I) iodide (19 mg, 0.1 mmol) in DMF (5 mL) was heated at 80 °C for 12 h under N_2 atmosphere. The reaction mixture was quenched with AcOEt and the suspension was filtered through Celite with AcOEt. After the organic layer was washed with water and dried over Na_2SO_4, the solvent was removed to give a residue. Column chromatography of the residue on silica gel under hexane/AcOEt (1:3) with Et_3N (1%) gave **7a** (150 mg, 49%) as a white powder; mp: 176–178 °C. ^{1}H NMR (300 MHz, $CDCl_3$) δ: 2.56 (3H, d, J = 1.8 Hz), 7.44–7.53 (m, 2H), 8.11 (1H, dt, J = 1.6, 8.3 Hz), 8.17–8.25 (4H, m), 8.47 (1H, d, J = 4.8 Hz), 8.96 (1H, dd, J = 1.5, 4.0 Hz). HRMS (FAB) calcd for $C_{17}H_{13}N_5F$: 306.1155; found: 306.1189 (M^+).

5.1.5. 6-[1-(2-Bromo-3-pyridyl)-5-methyl-1*H*-1,2,3-triazol-4-yl]quinoline (7b)

A mixture of **9b** (1.11 g, 2.1 mmol), **10** (554 mg, 2.0 mmol) and tetrakis(triphenylphosphine)palladium (0) (266 mg, 0.1 mmol), cesium fluoride (608 mg, 4.0 mmol), and copper (I) iodide (38 mg, 0.2 mmol) in DMF (5 mL) was heated at 80 °C for 12 h under N_2

atmosphere. The reaction mixture was quenched with AcOEt and the suspension was filtered through Celite with AcOEt. After the organic layer was washed with water and dried over Na_2SO_4, the solvent was removed to give a residue. Column chromatography of the residue on silica gel under hexane/AcOEt (1:3) with Et_3N (1%) gave **7b** (380 mg, 52%) as a white powder; mp: 163–165 °C. ^1H NMR (300 MHz, $CDCl_3$) δ: 2.52 (3H, s), 7.47 (1H, m), 7.57 (1H, m), 7.86 (1H, dd, J = 1.8, 7.7 Hz), 8.23–8.29 (4H, m), 8.65 (1H, dd, J = 1.8, 4.8 Hz), 8.96 (1H, dd, J = 1.5, 4.4 Hz). HRMS (FAB) calcd for $C_{17}H_{13}N_5Br$: 366.0354; found: 366.0363 (M^+).

5.2. Radiosynthesis

5.2.1. 6-[1-(2-[^{18}F]Fluoro-3-pyridyl)-5-methyl-1*H*-1,2,3-triazol-4-yl]quinoline ([^{18}F]FPTQ, [^{18}F]7a)

All synthetic sequences of [^{18}F]**7a** were carried out using a home-made automated synthesis system.[30] [^{18}F]F^- was produced by the ^{18}O (p, n) ^{18}F reaction on 95 atom% $H_2{}^{18}O$ using 18 MeV protons (14.2 MeV on target) from the cyclotron and separated from [^{18}O]H_2O using Dowex 1-X8 anion exchange resin. The [^{18}F]F^- was eluted from the resin with aqueous K_2CO_3 (3.3 mg/300 μL) into a vial containing a solution of 4,7,13,16,21,24-hexaoxa-1,10-diazabicyclo[8,8,8]hexacosane (Kryptofix 222, 25 mg) in CH_3CN (1.5 mL) and transferred into another reaction vessel in the hot cell.

The [^{18}F]F^- solution was dried to remove H_2O and CH_3CN at 120 °C for 15 min. After the dryness, a solution of **7b** (1 mg) in anhydrous DMSO (300 μL) was heated with [^{18}F]F^- at 150 °C for 10 min. The [^{18}F]fluorinating reaction was terminated by adding CH_3OH/50 mM $CH_3CO_2NH_4$ (4:6, 500 μL) and this mixture was applied to a semi-preparative HPLC system. HPLC purification was completed on a Fluofix 120 N C_{18} column (10 mm × 250 mm; Wako Pure Chem Ind, Osaka, Japan) using a mobile phase of CH_3OH/50 mM $CH_3CO_2NH_4$ (4:6) at a flow rate of 5.0 mL/min. The retention time for [^{18}F]**7a** was 23.5 min, whereas that for **7b** was 19.6 min. The radioactive fraction corresponding to [^{18}F]**7a** was collected in a sterile flask containing polysorbate 80 (100 μL) and 25% ascorbic acid (100 μL), evaporated to dryness under vacuum, re-dissolved in 3 mL sterile saline, and passed through a 0.22 μm Millipore filter to obtain the final product. At EOS, 1280–1830 MBq of [^{18}F]**7a** was obtained as an intravenously injectable solution at a beam current of 15 mA and 10 min proton bombardment from 3300–4000 MBq of [^{18}F]F^-.

Radioactive [^{18}F]**7a** was analyzed by radio-HPLC coupled with a UV detector to determine the radiochemical purity and specific activity (Fluofix 120 N C_{18}, 4.6 mm × 250 mm; $CH_3CN/H_2O/Et_3N$ = 1:1:0.05%, 0.8 mL/min, 11.2 min). The specific activity of [^{18}F]**7a** was calculated by comparing the assayed radioactivity to the mass associated with the carrier UV peak at 254 nm.

5.3. Measurement of partition coefficients (Log *D*)

Partition coefficient values were measured by mixing [^{18}F]**7a** (radiochemical purity: 100%; about 150,000 cpm) with *n*-octanol (3.0 g) and sodium phosphate buffer (PBS, 3.0 g; 0.1 M, pH 7.40) in a test tube. The tube was vortexed for 3 min at room temperature, followed by centrifugation at 3500 rpm for 5 min. An aliquot of 1 mL PBS and 1 mL *n*-octanol was removed, weighted, and counted, respectively. Samples from the remaining organic layer were removed and re-partitioned until consistent Log *D* values were obtained. The Log *D* value was calculated by comparing the ratio of cpm/g of *n*-octanol to that of PBS and expressed as Log *D* = Log[cpm/g (*n*-octanol)/cpm/g(PBS)]. All assays were performed in triplicate. Meanwhile, the values of *c* Log *D* and *c* Log *P* of [^{18}F]**7a** were computed using Pallas 3.4 software (CompuDrug; Sedona, AZ).

5.4. In vitro autoradiography

Four rat brains were quickly removed and frozen on powdered dry ice. Brain sagittal sections (20 mm) were cut on a cryostat microtome (HM560; Carl Zeiss, Germany) and thaw-mounted on glass slides, which were then dried and stored at −80 °C until used for experiments. Brain sections were preincubated (3´ 5 min) in Tris–HCl (50 mM, pH 7.4, containing 1.2 mM $MgCl_2$ and 2 mM $CaCl_2$) at room temperature. After preincubation, these sections were incubated for 30 min at room temperature in fresh buffer with [^{18}F]**7a** (0.023 nM, 0.3 MBq/200 mL). Unlabeled **7a** or **2** (1 mM) was used to determine the specific binding of [^{18}F]**7a** for mGluR1. Subgroup selectivity was investigated by MPEP (1 and 10 mM). After incubation, the sections were washed (3 × 5 min) with cold buffer, dipped in cold distilled water, and dried with cold air. These sections were placed in contact with imaging plates (BAS-MS2025; FUJIFILM, Tokyo, Japan). Autoradiograms were obtained and photo-stimulated luminescence values (PSL) in the regions of interest (ROIs) were measured using a Bio-Imaging Analyzer System (BAS5000, FUJIFLIM). Radioactivity concentrations in ROIs were expressed as PSL/area (mm^2) and calculated by subtracting the background (1.5 PSL/mm^2).

5.5. Biodistribution by dissection

A saline solution of [^{18}F]**7a** (average of 17 MBq/200 μL, 0.11 nmol) was injected into rats through the tail vein. Three rats for each time point were sacrificed by cervical dislocation at 5, 15, and 30 min after injection. Whole brain, lung, heart, liver, kidney, spleen, pancreas, muscle, small intestine, bone and blood samples were quickly removed and weighed. From the brain hemispheres, cerebellum, olfactory bulb, striatum, hippocampus, thalamus, pons-medulla, and cerebral cortex were further dissected and weighed. The radioactivity in these tissues was measured with a 1480 Wizard autogamma counter (Perkin–Elmer; Tokyo, Japan) and expressed as a percentage of the injected dose per gram of wet tissue (% ID/g). All radioactivity measurement was corrected for decay.

5.6. Small-animal PET imaging

Anatomical template images of rat brain were generated by a high-resolution magnetic resonance imaging (MRI) system.[25] Briefly, a rat was anesthetized with sodium pentobarbital (50 mg/kg, ip), and scanned with a 400 mm bore, 7 T horizontal magnet (NIRS/KOBELCO, Kobe; Japan/Bruker BioSpin, Ettlingen, Germany) equipped with 120 mm diameter gradients (Bruker BioSpin). A 72 mm diameter coil was used for radiofrequency transmission, and signals were received by a 4-channel surface coil. Coronal T2-weighted MRI images were obtained by a fast spin-echo sequence with the following imaging parameters: repetition time = 8000 ms, effective echo time = 15 ms, field of view (FOV) = 35 mm´ 35 mm, and slice thickness = 0.6 mm.

PET scans were performed using a small-animal Inveon PET scanner (Siemens Medical Solutions USA, Knoxville, TN), which provides 159 transaxial slices 0.796 mm (center-to-center) apart, a 10 cm transaxial FOV, and a 12.7 cm axial FOV. Before scans, the rats were anesthetized with 5% (v/v) isoflurane, and maintained thereafter by 1–2% (v/v) isoflurane. Emission scans were acquired for 60 min in 3-dimensional list-mode with an energy window of 350–750 keV, immediately after intravenous injection of [^{18}F]**7a** (16–18 MBq/200 mL, 0.07–0.11 nmol). To determine in vivo specific binding, unlabeled **7a**, **2**, or MPEP (1 mg/kg dissolved in 300 mL saline containing 10% ethanol and 5% polysorbate 80) was injected at 1 min before injection of [^{18}F]**7a**. Four rats were used for each experiment. All list-mode acquisition data were

sorted into 3-dimensional sinograms, which were then Fourier rebinned into 2-dimensional sinograms (frames × min: 4 × 1, 8 × 2, 8 × 5). Dynamic images were reconstructed with filtered back-projection using a Hanning's filter, a Nyquist cutoff of 0.5 cycle/pixel. ROIs were placed on the striatum, hippocampus, cerebral cortex, thalamus, medulla, and cerebellum using ASIPro VM™ (Analysis Tools and System Setup/Diagnostics Tool, Siemens Medical Solutions USA) with reference to the MRI template. Brain uptake of radioactivity was decay-corrected to the injection time and was expressed as the standardized uptake value (SUV), which was normalized to the injected radioactivity and body weight. SUV = (radioactivity per milliliter tissue/injected radioactivity) × gram body weight.

5.7. Protein binding

Plasma protein binding was determined by the ultra-filtration method using a Centrifree YM-30 filter unit (Millipore; Carrigtwohill, Ireland) according to a previously described method.[31] A blood sample (1.0 mL) was obtained from rats (n = 3) and was maintained at 37 °C in a centrifuge tube. Then, [^{18}F]**7a** (5 mL, approximately 10 Bq) was added and mixed in the blood sample. An aliquot (20 mL) of blood sample was taken to measure radioactivity in the sample using the autogamma counter. The remainder of blood sample was centrifuged at 3900 rpm for 5 min at 4 °C to obtain plasma. The plasma sample (40 mL) was loaded into the filter unit and centrifuged at 2000 rpm for 15 min at 25 °C. The remainder of plasma sample (20 mL) was used for measurement. An aliquot (100–150 mL) was taken from the ultrafiltrate and radioactivity was measured. The amount of nonspecific binding of [^{18}F]**7a** to the filter was also determined by adding [^{18}F]**7a** to saline and following the same procedure as for the plasma sample. The free fraction in plasma was calculated as the ratio of radioactivity in ultrafiltrate to radioactivity in plasma corrected for a stick factor. The stick factor is radioactivity in a known volume of ultrafiltered saline divided by radioactivity in the same volume of saline.

5.8. Metabolite assay for mouse plasma and brain tissue

After intravenous injection of [^{18}F]**7a** (3.7 MBq/100 μL) into ddy mice (n = 3), these mice were sacrificed by cervical dislocation at 5, 15, and 30 min. Blood (500 mL) and whole brain samples were removed quickly. The blood sample was centrifuged at 15,000 rpm for 2 min at 4 °C to separate plasma, which (250 μL) was collected in a test tube containing CH_3CN (500 μL) and a solution of unlabeled **7a** (0.8 mg/5.0 mL of CH_3CN, 10 μL). After the tube was vortexed for 15 s and centrifuged at 15,000 rpm for 2 min for deproteinization, the supernatant was collected. The extraction efficiency of radioactivity into the CH_3CN supernatant ranged from 70% to 92% of the total radioactivity in the plasma. On the other hand, the cerebellum and brain except the cerebellum were dissected from the mouse brain and homogenized together in an ice-cooled CH_3CN/H_2O (1:1, 1.0 mL) solution, respectively. The homogenate was centrifuged at 15,000 rpm for 2 min at 4 °C and supernatant was collected. The recovery of radioactivity into the supernatant was 68–87% based on the total radioactivity in the brain homogenate.

An aliquot of the supernatant (100–500 μL) obtained from the plasma or brain homogenate was injected into the radio-HPLC system, and analyzed under the same analytical conditions described above except that the mobile phase was CH_3CN/H_2O (4:6) and flow rate was 1.5 mL/min. The percentage rate of [^{18}F]**7a** to total radioactivity (corrected for decay) on the HPLC chromatogram was calculated as% = (peak area for [^{18}F]**7a**/total peak area) × 100.

Acknowledgments

We thank the crew of the Cyclotron Operation Section and Molecular Imaging Center of National Institute of Radiological Sciences for support in operation of the cyclotron, production of radioisotope, and animal experiments.

Supplementary data

Supplementary data associated with this article can be found, in the online version, at doi:10.1016/j.bmc.2010.11.048.

References and notes

1. Nakanishi, S. *Neuron* **1994**, *13*, 1031.
2. Conn, P. J.; Pin, J. P. *Annu. Rev. Pharmacol. Toxicol.* **1997**, *37*, 205.
3. Ferraguti, F.; Crepaldi, L.; Nicoletti, F. *Pharmacol. Rev.* **2008**, *60*, 536.
4. Bordi, F.; Ugolini, A. *Prog. Neurobiol.* **1999**, *59*, 55.
5. Kew, J. N. *Pharmacol. Ther.* **2004**, *104*, 233.
6. Swanson, C. J.; Bures, M.; Johnson, M. P.; Linden, A. M.; Monn, J. A.; Schoepp, D. D. *Nat. Rev. Drug Discovery* **2005**, *4*, 131.
7. Vanejevs, M.; Jatzke, C.; Renner, S.; Müller, S.; Hechenberger, M.; Bauer, T.; Klochkova, A.; Pyatkin, I.; Kazyulkin, D.; Aksenova, E.; Shulepin, S.; Timonina, O.; Haasis, A.; Gutcaits, A.; Parsons, C. G.; Kauss, V.; Weil, T. *J. Med. Chem.* **2008**, *51*, 634.
8. Schkeryantz, J. M.; Kingston, A. E.; Johnson, M. P. *J. Med. Chem.* **2007**, *31*, 2563.
9. Litschig, S.; Gasparini, F.; Rueegg, D.; Stoehr, N.; Flor, P. J.; Vranesic, I.; Prézeau, L.; Pin, J. P.; Thomsen, C.; Kuhn, R. *Mol. Pharmacol.* **1999**, *55*, 453.
10. Carroll, F. Y.; Stolle, A.; Beart, P. M.; Voerste, A.; Brabet, I.; Mauler, F.; Joly, C.; Antonicek, H.; Bockaert, J.; Müller, T.; Pin, J. P.; Prézeau, L. *Mol. Pharmacol.* **2001**, *59*, 965.
11. Lavreysen, H.; Janssen, C.; Bischoff, F.; Langlois, X.; Leysen, J. E.; Lesage, A. S. *Mol. Pharmacol.* **2003**, *63*, 1082.
12. Kohara, A.; Toya, T.; Tamura, S.; Watabiki, T.; Nagakura, Y.; Shitaka, Y.; Hayashibe, S.; Kawabata, S.; Okada, M. *J. Pharmacol. Exp. Ther.* **2005**, *315*, 163.
13. Wu, W. L.; Burnett, D. A.; Domalski, M.; Greenlee, W. J.; Li, C.; Bertorelli, R.; Fredduzzi, S.; Lozza, G.; Veltri, A.; Reggiani, A. *J. Med. Chem.* **2007**, *50*, 5550.
14. Satoh, A.; Nagatomi, Y.; Hirata, Y.; Ito, S.; Suzuki, G.; Kimura, T.; Maehara, S.; Hikichi, H.; Satow, A.; Hata, M.; Ohta, H.; Kawamoto, H. *Bioorg. Med. Chem. Lett.* **2009**, *19*, 5464.
15. Huang, Y.; Narendran, R.; Bischoff, F.; Guo, N.; Zhu, Z.; Bae, S. A.; Lesage, A. S.; Laruelle, M. *J. Med. Chem.* **2005**, *48*, 5096.
16. Lavreysen, H.; Wouters, R.; Bischoff, F.; Nóbrega Pereira, S.; Langlois, X.; Blokland, S.; Somers, M.; Dillen, L.; Lesage, A. S. *Neuropharmacology* **2004**, *47*, 961.
17. Fotuhi, M.; Sharp, A. H.; Glatt, C. E.; Hwang, P. M.; von Krosigk, M.; Snyder, S. H.; Dawson, T. M. *J. Neurosci.* **1993**, *13*, 2001.
18. Lavreysen, H.; Pereira, S. N.; Leysen, J. E.; Langlois, X.; Lesage, A. S. *Neuropharmacology* **2004**, *46*, 609.
19. Eng, W.; Kawamoto, H.; O'Malley, S.; Krause, S.; Patel, S.; Ryan, C.; Riffel, K.; Ito, S.; Suzuki, G.; Cook, J.; Ozaki, S.; Ohta, H.; Burns, D.; Hargreaves, R.; Hostetler, E. *J. Labelled Compd. Radiopharm.* **2009**, *52*, S84.
20. Suzuki, G.; Kimura, T.; Satow, A.; Kaneko, N.; Fukuda, J.; Hikichi, H.; Sakai, N.; Maehara, S.; Kawagoe-Takaki, H.; Hata, M.; Azuma, T.; Ito, S.; Kawamoto, H.; Ohta, H. *J. Pharmacol. Exp. Ther.* **2007**, *321*, 1144.
21. Ohgami, M.; Haradahira, T.; Takai, N.; Zhang, M.-R.; Kawamura, K.; Yamasaki, K.; Yanamoto, K. *Eur. J. Nucl. Med. Mol. Imag.* **2009**, *36*, S310.
22. Hostetler, E.; Eng, W.; Joshi, A.; Sanabria-Bohórquez, S.; Kawamoto, H.; Ito, S.; O'Malley, S.; Krause, S.; Ryan, C.; Patel, S.; Williams, M.; Riffel, K.; Suzuki, G.; Ozaki, S.; Ohta, H.; Cook, J.; Burns, H. D.; Hargreaves, R. *Synapse* **2010**. doi:10.1002/syn.20826.
23. Prabhakaran, J.; Majo, V. J.; Milak, M. S.; Kassir, S. A.; Palner, M.; Savenkova, L.; Mali, P.; Arango, V.; Mann, J. J.; Parsey, R. V.; Kumar, J. S. *Bioorg. Med. Chem. Lett.* **2010**, *20*, 3499.
24. Kohara, A.; Takahashi, M.; Yatsugi, S.; Tamura, S.; Shitaka, Y.; Hayashibe, S.; Kawabata, S.; Okada, M. *Brain Res.* **2008**, *1191*, 168.
25. Yanamoto, K.; Konno, F.; Odawara, C.; Yamasaki, T.; Kawamura, K.; Hatori, A.; Yui, J.; Wakizaka, K.; Nengaki, N.; Takei, M.; Zhang, M.-R. *Nucl. Med. Biol.* **2010**, *37*, 615.
26. Kawamoto, H.; Ito, S.; Satoh, A.; Nagatomi, Y.; Hirada, Y.; Kimura, T.; Suzuki, G.; Sato, A.; Ohta, H. WO 2005/085214 A1, 2005.
27. Suzuki, G.; Kawagoe-Takaki, H.; Inoue, T.; Kimura, T.; Hikichi, H.; Murai, T.; Satow, A.; Hata, M.; Maehara, S.; Ito, S.; Kawamoto, H.; Ozaki, S.; Ohta, H. *J. Pharmacol. Sci.* **2009**, *110*, 315.
28. Pike, V. W. *Trends Pharmacol. Sci.* **2009**, *30*, 431.
29. Zhang, M.-R.; Maeda, J.; Ogawa, M.; Noguchi, J.; Ito, T.; Yoshida, Y.; Okauchi, T.; Obayashi, S.; Suhara, T.; Suzuki, K. *J. Med. Chem.* **2004**, *47*, 2228.
30. Fukumura, T.; Suzuki, H.; Mukai, K.; Zhang, M.-R.; Yoshida, Y.; Nemoto, K.; Suzuki, K. *J. Labelled Compd. Radiopharm.* **2007**, *50*, S202.
31. Kawamura, K.; Naganawa, M.; Konno, F.; Yui, J.; Wakizaka, H.; Yamasaki, T.; Yanamoto, K.; Hatori, A.; Takei, M.; Yoshida, Y.; Sakaguchi, K.; Fukumura, T.; Kimura, Y.; Zhang, M.-R. *Nucl. Med. Biol.* **2010**, *37*, 625.